

A new view of macula densa cell microanatomy

Georgina Gyarmati,¹ Urvi Nikhil Shroff,¹ Anne Riquier-Brison,¹ Wilhelm Kriz,² Brigitte Kaissling,³ Christopher R. Neal,⁴ Kenton P. Arkill,⁵ Nariman Ahmadi,⁶ Inderbir S. Gill,⁶ Ju-Young Moon,¹ Dorinne Desposito,¹ and János Peti-Peterdi¹

¹Departments of Physiology and Neuroscience, and Medicine, Zilkha Neurogenetic Institute, University of Southern California, Los Angeles, CA 90033

²Centre for Biomedicine and Medical Technology Mannheim (CBTM), Neuroanatomy, Medical Faculty Mannheim, Heidelberg University, Mannheim, Germany

³Institute of Anatomy, University of Zurich, Zurich Switzerland

⁴Bristol Renal, Bristol Heart Institute, Translational Health Sciences, Bristol Medical School, University of Bristol, Bristol, U.K.

⁵Division of Cancer and Stem Cells, School of Medicine, University of Nottingham Biodiscovery Institute, Science Road, University Park, NG7 2RD, UK.

⁶Institute of Urology, Catherine & Joseph Aresty Department of Urology, Keck School of Medicine, University of Southern California, Los Angeles, CA

Running head: Macula densa basal cell processes Word count: Abstract 250, Main text: 3304

Supplemental Material available at

DOI: <https://doi.org/10.6084/m9.figshare.11983791.v1>

Corresponding author: J Peti-Peterdi, Dept. of Physiology and Neuroscience, Zilkha Neurogenetic Institute, University of Southern California, 1501 San Pablo Street, ZNI 335, Los Angeles, California 90033, E-mail: petipete@usc.edu

Abstract

Although macula densa (MD) cells are chief regulatory cells in the nephron with unique microanatomical features, they have been difficult to study in full detail due to their inaccessibility and limitations in earlier microscopy techniques. The present study used a new mouse model with a comprehensive imaging approach to visualize so far unexplored microanatomical features of MD cells, their regulation and functional relevance. MD-GFP mice with conditional and partial induction of green fluorescent protein (GFP) expression, which specifically and intensely illuminated only single MD cells were used with fluorescence microscopy of fixed tissue and live MD cells in vitro and in vivo with complementary electron microscopy (EM) of rat, rabbit, and human kidney. An elaborate network of major and minor cell processes here named maculapodia were found at the cell base, projecting towards other MD cells and the glomerular vascular pole. The extent of maculapodia showed up-regulation by low dietary salt intake and female gender. Time-lapse imaging of maculapodia revealed highly dynamic features including rapid outgrowth and an extensive vesicular transport system. EM of rat, rabbit, and human kidneys, and three-dimensional (3D) volume reconstruction in optically cleared whole-mount MD-GFP mouse kidneys further confirmed the presence and projections of maculapodia into the extraglomerular mesangium and the afferent and efferent arterioles. The newly identified dynamic and secretory features of MD cells suggest the presence of novel functional and molecular pathways of cell-to-cell communication in the juxtaglomerular apparatus (JGA) between MD cells and between MD and other target cells.

Keywords: macula densa, microanatomy, PAPP2, paracrine signaling, gender specificity

Introduction

The macula densa (MD) is a plaque of 20-25 highly specialized and polarized renal epithelial cells in each nephron at the distal end of the thick ascending limb, strategically localized at the glomerular vascular pole as the tubular component of the juxtaglomerular apparatus (JGA). Their basal cell surface is facing and is in direct contact with the vascular component of the JGA, including vascular smooth muscle cells of the afferent (AA) and efferent (EA) arterioles, renin producing juxtaglomerular (JG) and extraglomerular mesangial cells. The unique MD cell microanatomy, including prominent primary cilia at the luminal membrane (7, 31, 36) apically localized cell nuclei, and various organelles involved in the MD protein and autacoid synthetic machinery packed in the basal part of the cell body has been long recognized, and linked to the functional role of the MD in sensing the local tissue environment and signaling to the JGA (2, 6, 10, 24, 29). In fact, the special features of these organelles play important roles in the traditional functions of the MD to sense alterations in tubular salt and other factors of the local tissue environment and to translate that information to the synthesis and release of various chemical mediators through their basal membrane for paracrine cell-to-cell crosstalk with other JGA cell types (3, 6, 24, 29). On the whole cell and physiological level, via these features MD cells regulate renal and glomerular hemodynamics via tubuloglomerular feedback, and the release of renin from adjacent juxtaglomerular (JG) cells (6, 24, 29).

MD cells are thought to communicate with their neighbor JGA cells via humoral mediators released extracellularly through their basolateral cell membrane and the very thin and fragmented basement membrane, and in the absence of significant direct physical cell-to-cell contact such as gap junctions (33, 37). Tiny processes of the MD cell basal membrane protruding towards the

mesangium have been described earlier based on electron microscopy of fixed kidney specimen (3, 5, 10) including a recent report on human MD (7). However, the full extent and dynamic features of these basal processes have been unknown due to the complex 3D structure of the JGA and inherent limitations in past histology techniques. Recently, new fluorescence imaging techniques and genetic mouse models have been developed that allow cell membrane targeting of highly fluorescent marker proteins (14, 25, 27). These approaches have helped to label and visualize fine details of cell membranes including podocyte foot processes (13) and in vivo approaches (15) using optical microscopy.

The purpose of the present study was to visually characterize and analyze the morphological and dynamic features of MD cell microanatomy using novel fluorescence imaging tools, with particular emphasis on the critically important, but most inaccessible basal cell processes.

Materials and Methods

Animals and Kidney Tissues

All animal protocols were approved by the Institutional Animal Care and Use Committee at the University of Southern California. Male and female, 6-8 weeks-old C57BL6/J mice (Jackson Laboratory, Bar Harbor, ME) were used in all experiments. Tamoxifen-inducible, conditional MD-GFP mice on C57BL6/J background were generated by intercrossing nNOS/CreERT2 and mTmG/fl mice as described previously (both from Jackson Laboratory) (27). The mTmG reporter mice contain a myristoylated and palmitoylated 41 amino acid N-terminal MARCKS membrane tag for efficient membrane targeting as described before (22). Tamoxifen was administered 75 mg/kg by oral gavage only once for partial induction, and for a total of three times (every other day) for full induction. Some mice received low-salt diet for 10 to 14 days (TD 90228, Harlan Teklad, Madison, WI) combined with ACE inhibitor treatment using enalapril (150 mg/L via drinking water, purchased from Sigma, St. Louis, MO), or high salt diet (4% NaCl, TD110078 from Harlan Teklad). For immunohistochemical analysis, anonymized, human adult (32-87 years old) formalin-fixed paraffin-embedded renal cortical tissues were obtained from unaffected regions of tumor nephrectomy specimens (HS-15-00298 and HS-16-00378 protocols approved by the Institutional Review Board, Keck School of Medicine of the University of Southern California). Basic patient history data regarding the presence of chronic kidney disease (CKD) and comorbidities, such as hypertension, diabetes, were available. Only samples with no history of CKD and diabetes were included in this study. For serial block face scanning electron microscopy, human kidney tissue was obtained with

appropriate consent and after review by UK research ethics committee (study approval 07/H0102/45) in accordance with UK legislation and the Helsinki Declaration.

Immunohistochemistry of fixed kidney tissue

Immunofluorescence detection of proteins was performed as described previously (27). Briefly, kidneys were perfused and fixed in 4% PFA for 2 hours at room temperature, embedded in paraffin, and sectioned 8 μm thick. For antibody stains, slides were washed in 1XPBS. For antigen retrieval, heat-induced epitope retrieval was applied by boiling sections in Sodium Citrate buffer (pH 6.0) or Tris-EDTA (pH 9.0) for ten minutes. To reduce non-specific binding, sections were blocked with normal goat serum (1:20). Primary and secondary antibodies were applied sequentially overnight at 4° C and 2 hours at room temperature. Primary antibodies and dilutions were as follows: nNOS (Santa Cruz Biotechnology, Santa Cruz, CA, 1:100), alpha-Tubulin and PAPP2 (Thermo Fisher Scientific, Waltham, MA, 1:100), renin (AS-54371, AnaSpec Inc 1:100), GFP (ThermoFisher,1:200). Alexa Fluor 488, 594, and 647-conjugated secondary antibodies and Alexa Fluor 680-Phalloidin were purchased from Thermo Fisher Scientific. In some experiments the primary PAPP2 antibody was preincubated with the immunizing (blocking) peptide per manufacturer's instructions (Thermo Fisher Scientific). Slides were mounted by using DAPI-containing mounting media (VectaShield, Vector Laboratories Inc., Burlingame, CA). The immunohistochemistry images for Actin-associated proteins Rho Guanine Nucleotide Exchange Factor 25 (ARHGEF25) and Actin Related Protein 2/3 Complex Subunit 1A (ARPC1A), as well as the Cilia and Flagella Associated Protein 36 (CFAP36) and Intraflagellar Transport (IFT) associated protein IFT43 were obtained from the Human Protein

Atlas (<http://www.proteinatlas.org>) that were obtained with antibodies that have not been fully validated in the current studies (34).

For structural analysis of MD cell major processes, 20 μm thick frozen sections and endogenously expressed genetic reporter (GFP) imaging were used. Sections were washed in PBS and mounted with DAPI-containing mounting media. High spatial resolution Z-stack recordings and maximum intensity projection images (MIP) were used to measure the length of basal cell processes. Only superficial cortical nephrons were selected, and the longest process per individual MD cell was included in the blind morphometric analysis. The sections were identified by animal number only rather than by experimental groups, which were unknown to the examiner. Sections were examined with Leica TCS SP5 and SP8 DIVE (Leica Microsystems, Wetzlar, Germany) confocal/multiphoton laser scanning microscope systems as described previously (27, 28, 30). Imaris 9.2 image analysis software was used for 3D reconstruction modeling.

Multiphoton microscopy (MPM) of live MD cells in vivo and in vitro

MD-GFP mice were anesthetized and intravital imaging of the intact living kidney was performed using a Leica SP8 DIVE multiphoton microscope (MPM) (Leica Microsystems, Wetzlar, Germany) powered by a Discovery laser system (Coherent Inc., Santa Clara, CA) as described previously (15, 28, 30). For imaging live MD cells in vitro, MD-GFP mice were perfused through the left ventricle with ice cold PBS, and the kidneys were harvested. Freshly isolated and in vitro microperfused JGA preparations from superficial cortical nephrons with attached glomeruli were used as before (23). For isolation of single live MD cells, kidney cortex was isolated and digested using Hyaluronidase and Liberase TM enzyme combination (concentration: 2mg/mL and 2.5mg/mL respectively, from Sigma). After digestion, MD and

control cells were isolated based on their genetic reporter expression (GFP or tdTomato) by using FACS ARIALL cell sorter at 4°C, and excitation wavelengths 488 and 633nm in sterile conditions. Subsequently, the freshly isolated single living MD cells were immediately transferred to a glass coverslip-bottomed chamber and bathed in culture media (DMEM mixture F12, pH 7.4) at room temperature and no-flow conditions. High temporal and spatial resolution fluorescence imaging was performed to visualize the microanatomical features as described before (23, 27) using a Leica TCS SP5 multiphoton confocal laser scanning microscope system (Leica Microsystems, Wetzlar, Germany). Z-stack recordings and MIP images of single MD cells were used to identify the number of minor cell processes per cell. Some coverslips with attached MD cells were subsequently processed for PFA fixation (at room temperature for 10 minutes) and immunofluorescence labeling as described above.

Tissue CLARITY

Three-dimensional imaging was performed as previously described (21) by carrying out whole-mount immunofluorescence stains on slices of MD-GFP mouse kidneys. Slices were fixed in 4% formaldehyde in 1x phosphate buffer saline (PBS) at room temperature for 45 min, washed in 1XPBS, blocked in 1xPBS with 0.1% TritonX100 and 2% SEA Block (Thermo Fisher Scientific) for 1 hour, and sequentially incubated in primary and secondary antibodies over 2 days. Primary and secondary antibodies were diluted in the blocking solution. To clear tissue slices, the slices were dehydrated in methanol via increasing concentrations 50%, 75%, 100%, diluted in PBS - each for 1hr - and subsequently submerged in a 50:50 benzyl benzoate/benzyl alcohol (BABB): methanol solution, followed by 100% BABB. High resolution imaging of MD plaques and the adjacent glomeruli was performed on a Leica SP8 multiphoton microscope using

a 63X glycerol immersion objective (NA 1.3). 3D reconstruction and surface rendering was performed as described previously (11). Briefly, high temporal resolution Z-stack recording of MD plaques (63X magnification, 0.2 μm z-step size) was used and processed by Imaris 9 surface rendering technology. To create a 3D surface defining the morphology of MD cells including the fine details of basal processes, membrane-targeted GFP fluorescence of MD cells was used as the source channel. Using surface rendering, fluorescence thresholding and masking, the accurate 3D structure of individual MD plaques and cells was obtained including the number and orientation of major and minor basal cell processes.

Transmission electron microscopy (TEM)

Kidneys were fixed via total body perfusion as described previously (16). Without prior flushing, the animals were directly perfused with 2% glutaraldehyde phosphate buffer solution (GA-PBS) supplemented with 0.05% citric acid (pH 7.5, 485 mOsmol/L) at a constant pressure of 100 mmHg for 3 minutes. Kidney slices were postfixated in 2% GA-PBS overnight, and in 1% OsO_4 for 2 hours, and subsequently dehydrated and embedded into epon by standard procedures. Ultrathin sections of selected areas were cut on ultracut microtome (Leica Nußloch, Germany) using a diamond knife and studied with transmission electron microscopy (TEM) as described before (16).

Serial Block Face Scanning Electron Microscopy (SBF-SEM)

Human tissue blocks were prepared from unused transplant kidneys by perfusion fixation combined with additional aqueous heavy metal steps as described previously (1). Briefly, trimmed mounted block with the region of interest was attached to the chuck and the resin

embedded glomeruli with the adjacent MD were sectioned using a Gatan 3view ultramicrotome within a FEI Quanta 250 scanning electron microscope (SBF-SEM). Once the surface was imaged, an automatic routine advanced the specimen and sectioned the block face removing a 150nm thick resin section. The sequence of advance was repeated until all images were acquired.

Statistical methods

Data are expressed as average \pm SEM and were analyzed using Student's t-tests (between two groups), or ANOVA (for multiple groups) with post-hoc comparison by Bonferroni test. $P < 0.05$ was considered significant. Statistical analyses were performed using GraphPad Prism 7.0c (GraphPad Software, Inc.).

Results

Histological features of the MD-GFP mouse model

Using the classic MD cell-specific marker nNOS in a Cre/lox-based genetic strategy, MD-GFP mice were generated by intercrossing nNOS/CreERT2 and mTmG/fl mice as described recently (27). These mice feature MD-specific, tamoxifen-inducible membrane-targeted enhanced green fluorescent protein (eGFP) expression in the renal cortex, while other cell types remain red by expressing the membrane-targeted red fluorescent protein tdTomato (Fig. 1A). To confirm the MD cell-specific, nNOS-driven expression of membrane targeted eGFP (mG) in MD-GFP mice, immunofluorescence double labeling of nNOS and eGFP was performed (Figure 1B). The overlay in Figure 1B shows co-labeling of nNOS and eGFP only in MD cells, confirming the validity and specificity of the applied genetic approach.

Next, tamoxifen dosing was adjusted to alter the level of Cre induction and hence the density of GFP-labeled MD cells in the renal cortex. Fig. 1C shows labeling of the entire MD plaque after full induction (75mg/kg tamoxifen via oral gavage given every other day for a total of three times), while partial induction (75mg/kg tamoxifen via oral gavage only once) led to sporadic MD cell labeling, only 1 to 3 MD cells/ plaque on average (Figs. 1D, 2-3). As a result of the membrane-targeting genetic fluorescence labeling approach, it became possible to visualize the fine morphological details of MD cell membrane structures, such as the primary cilia at the MD cells' apical membrane (Fig. 2C). Importantly, the combination of membrane-targeted fluorescence reporter expression with the sporadic labeling of single MD cells enabled the visualization of the microanatomical details of MD cells, and depicted an elaborate network of major and minor processes at the cell base, projecting towards the glomerulus and other MD cells

(Fig. 1D). We named these structures maculapodia, based on their foot-like projections from the MD cell body at their basal region.

Morphological analysis of MD cell major processes

To characterize the size of the cell processes network at the MD cell basal region, morphological analysis was performed first on fixed kidney sections to measure the length of major processes. Major processes were defined as a few primary (projecting directly from the cell body, 1-3 on average) and thick (>0.5 - $1.0\ \mu\text{m}$) cytoplasmic protrusions from the MD cell basal region. Histological analysis confirmed that most MD cells under all conditions have visible major cell protrusions at their base running in parallel with the tubular side of the basement membrane, or crossing through the fragmented basement membrane towards other MD cells, the extraglomerular mesangium, the AA and EA. In control, the length of major processes was $4.63\pm 0.21\ \mu\text{m}$ on average ($n=8$ mice), but were occasionally seen to extend up to $14\ \mu\text{m}$ (Figs. 2A-G). Interestingly, we found that female mice had significantly longer major processes ($5.68\pm 0.32\ \mu\text{m}$) as compared to male littermates ($3.76\pm 0.22\ \mu\text{m}$, $p=0.001$, $n=4$ each), as shown in Figs. 2A, D, G, and Supplemental Video S1. Although only superficial cortical nephrons were included in all morphometric analysis, MD cells in inner cortical (juxtamedullary) nephrons appeared to have similar features (Fig. 2H).

Since tubular salt sensing and paracrine signaling to the JGA are well-known traditional functions of MD cells, we next applied various dietary salt intake manipulations to address the physiological regulation of MD cell microanatomy at the basal region. As shown in representative images and morphological analysis in Figs. 2A-F and G, the stimulation of MD cell salt sensing activity by combined low-salt diet and ACE inhibition resulted in the development of a more

elaborate maculapodia network in male mice, with a significant increase in the length of major processes ($5.01 \pm 0.34 \mu\text{m}$, $p=0.002$; $n=4$) (Fig. 2B, G). In contrast, high dietary sodium intake led to significant decrease in the length of these structures in both male and female mice ($1.94 \pm 0.22 \mu\text{m}$ in male, and $3.88 \pm 0.36 \mu\text{m}$ in female mice, $p=0.01$; $n=4-5$) (Fig. 2C, G). Furthermore, we found that the gender difference in the length of major processes was preserved in the condition of high dietary salt intake, while the gender difference disappeared under combined low-salt diet and ACE inhibition conditions due to significant changes in male but not in female mice (Fig. 2G).

Intravital imaging of maculapodia

To confirm the presence of MD cell major and minor processes in the intact living kidney tissue, low-salt diet and ACE inhibitor treated MD-GFP mice were used due to the presence of a more elaborate maculapodia network in this condition. We first performed multiphoton microscopy (MPM) of intact MD-GFP kidneys *in vivo*. Although motion artifacts due to vital functions made the visualization of minor processes difficult, several major MD cell processes were clearly observed projecting from the MD base into the extraglomerular mesangium and towards glomerular arterioles (Fig. 3A). In another approach of imaging intact living tissue, we next used the freshly dissected and *in vitro* microperfused JGA preparation from MD-GFP mice after partial tamoxifen induction. In contrast to the *in vivo* model, this was a perfectly steady preparation. Accordingly, both major ($0.5-1.0 \mu\text{m}$ thick and up to $34 \mu\text{m}$ long) and much thinner, hair-like minor MD cell basal processes were clearly observed forming a dense maculapodia network between individual MD cells and between MD and other JGA cells (Fig. 3B, and Supplemental Video S1, <https://doi.org/10.6084/m9.figshare.11983791.v1>). Minor processes were seen originating from either the cell body or major processes (Fig. 3B).

Quantitative visualization of structural and dynamic features of MD cell minor processes

Minor processes were defined as long, very thin ($<0.5\mu\text{m}$) hairlike cell processes projecting from either the cell body or major processes. To further elucidate their specificity, scale and dynamic features, living MD cells were freshly isolated from kidney tissue of MD-GFP mice on control and low-salt diet using FACS, and visualized by using high temporal and spatial resolution MPM imaging. As observed in fresh living tissues and histology sections (Figs. 1-3), high resolution MPM imaging of single living MD cells depicted a dense network of long, thin, hairlike minor processes (Fig. 4A). No major processes were seen in freshly isolated MD cells. The minor processes were preserved at the cells' basal region, and specific for MD cells based on the absence of such processes in control cells that were adjacent to the MD (Fig. 4B, and Supplemental Video S2, <https://doi.org/10.6084/m9.figshare.11983791.v1>). In control condition, MD cells from female mice had a higher number of minor processes (10.3 ± 1.4 per single MD cell) as compared to male littermates (4.8 ± 1.4 per single MD cell, $p<0.05$; $n=8-15$ MD cells from $n=3$ mice in each group) as shown in Fig. 4A, further strengthening the case that female mice have a more detailed maculapodia network. Physiological stimulation of MD cell salt sensing by combined low-salt diet with ACE inhibition resulted in significantly increased number of MD cell minor processes (14.5 ± 1.3 per single MD cell, $n=47$ MD cells from $n=7$ mice) as compared to control (8.4 ± 1.1 per single MD cell, $n=23$ MD cells from $n=6$ mice) (Fig. 4A). This increase was more pronounced in males (12.8 ± 1.5 per single MD cell, $n=29$ MD cells from $n=4$ mice) as compared to females (17.2 ± 2.1 per single MD cell, $n=18$ MD cells from $n=3$ mice).

Since actin and actin-associated proteins are common molecular building blocks of such cell processes, immunofluorescence labeling of freshly isolated, attached, and fixed MD cells was

performed which identified the presence of F-actin but not tubulin within the minor processes (Fig. 4C). In addition, immunoperoxidase labeling of human kidney sections (based on data obtained from the Human Protein Atlas) identified the high level and MD cell-specific basolateral expression of actin-associated proteins Rho Guanine Nucleotide Exchange Factor 25 (ARHGEF25) and Actin Related Protein 2/3 Complex Subunit 1A (ARPC1A), as well as well-known cilia and flagella associated proteins such as Cilia and Flagella Associated Protein 36 (CFAP36) and Intraflagellar Transport (IFT) associated proteins (e.g. IFT43). Besides the high level of expression of these actin-associated and microtubule proteins at the apical region that correlates with the previously characterized prominent primary cilia in MD cells (7, 31, 32, 36) and therefore serves as a positive control, a distinct basolateral expression was also detected suggesting their role in the structure and vesicular transport system of the MD cell basal processes network (Fig. 4C).

The expression of membrane-targeted eGFP in MD-GFP mice, and the MPM imaging approach enabled the high temporal and spatial resolution imaging of both plasma and intracellular membranes. Time-lapse imaging of single MD cells and their minor processes revealed the highly dynamic features of these long cell processes (Fig. 4D), such as their outgrowth or shortening in a few seconds (Fig. 4D, and Supplemental Video S3, <https://doi.org/10.6084/m9.figshare.11983791.v1>). In addition, multiple cytoplasmic vesicles were visible within minor processes and appeared rapidly moving in both directions between the cell body and their tip, suggesting their role in MD cell endocytosis and secretory functions (Fig. 4D, and Supplemental Video S4, <https://doi.org/10.6084/m9.figshare.11983791.v1>). To identify the potential cargo of such vesicles, immunostaining of Pregnancy-Associated Plasma Protein A2 (PAPPA2), a known secreted protease that has been used recently as a specific MD-distal tubule

marker (8, 20), was performed on human kidney sections and freshly isolated, attached and fixed MD cells from MD-GFP mice. Fig. 4D shows the high level of expression of PAPP2 in MD cells in a vesicular pattern within the cell body as well as at basal cell regions in the human kidney and within the cell processes of mouse MD cells (Fig. 4D). To confirm antibody specificity, the PAPP2 immunolabeling was lost after the primary antibody was pre-incubated with the immunizing (blocking) peptide (Fig. 4D).

Ultrastructural analysis of the MD cell basal region by TEM in multiple species

Transmission electron microscopy was performed to re-evaluate the ultrastructure of the MD basal anatomical region in the rabbit, rat, and human kidney. Besides the well-known unique features of MD cells, such as apically localized nuclei, and organelles involved in protein synthetic machinery packed in the basal part of the cell body, these experiments visualized and further confirmed that MD cells have prominent basal cell major and minor processes extending into the extraglomerular mesangium. The basal cell protrusions displayed fine ramifications, which seemed to interdigitate (Fig. 5A-D). Adjacent MD cells were seen interconnected by minor processes both at the basal and lateral membranes (Fig. 5C). The interface between the MD and the extraglomerular mesangium (EGM) in all species studied consisted of areas with many major and minor processes originating from MD cells that were intertwined with each other, partially separated by the fragmented and thin basement membrane material, and seemed to protrude into the EGM (Fig. 5A-E). Serial block-face scanning electron microscopy of human MD plaque and the adjacent glomerulus (Fig. 5E) confirmed the presence of a dense network of MD cell processes projecting into the EGM in close proximity to the efferent arteriole (Fig. 5E).

3D reconstruction of the MD cell basal processes (maculapodia) network

To visualize the three-dimensional structural features of mouse MD cells's basal region, MPM optical slicing was performed on immunofluorescence labeled whole kidney tissues of MD-GFP mice that were optically cleared using BABB CLARITY. Specifically, our focus was the features of the basal cell region and orientation, relative to the adjacent glomerulus, extraglomerular mesangium, the AA and EA. High-resolution optical slices clearly depicted the intercellular network of MD cell basal major and minor processes as shown in Fig. 6A-C. The reconstruction of MD cell basal cell membrane features in 3D confirmed the presence of cell-to-cell contacts between individual MD cells via major and minor processes within the same MD plaque (Fig. 6A, C). In addition, MD cell major and minor processes were detected projecting into the extraglomerular mesangium at the glomerular vascular pole, and closely wrapping around individual cells of the AA and EA (Fig. 6A,C, and Supplemental Video S5, <https://doi.org/10.6084/m9.figshare.11983791.v1>). To study the 3D spatial relation of MD cell processes and renin cells in the JGA, double labeling of MD cells and JG renin cells was performed on thick frozen sections of MD-GFP mouse kidney tissue. High spatial resolution Z-stack projection images were generated by using 3D surface rendering model. The results shown in Fig. 6C further confirmed the presence of a dense network of MD cell minor processes extending up to 30 μm long (Fig. 6C) towards the individual cells of the AA, EA and the surrounding EGM. Target cells that MD cells were making contact with via the major and minor processes included, but were not limited to, JG renin cells of the AA and EA (Fig. 6C, and Supplemental Video S6, <https://doi.org/10.6084/m9.figshare.11983791.v1>).

Discussion

The present study provided an unprecedented detailed view and comprehensive morphological analysis of the microanatomical features of the unique specialized renal epithelium of the macula densa, by taking advantage of recent developments in imaging, transgenic mouse, tissue processing and clearing technologies. Genetic labeling of single MD cells in MD-GFP mouse kidneys, and their high resolution MPM imaging *in vivo*, *in vitro*, in fixed thick sections, and after the fresh isolation of living MD cells uniformly found an elaborate network of major and minor processes at the cell base, projecting towards the glomerulus and other MD cells. Here we named these structures maculapodia, based on their foot-like appearance and projections from the base of the MD cell body. The extent of these basal cell processes showed regulation by dietary salt intake and gender specificity. Time-lapse imaging of MD minor processes revealed their highly dynamic features including rapid outgrowth and an extensive, including secretory vesicular transport system within these processes. Electron microscopy analysis in multiple species (rat, rabbit, human), and 3D image reconstruction of the JGA volume in optically cleared whole mount MD-GFP mouse kidneys further confirmed the presence of MD cell major and minor basal processes projecting into the extraglomerular mesangium at the glomerular vascular pole and the AA and EA. The highly elaborate network and physiological regulation of maculapodia, that contain various vesicles with secretory cargo (including PAPP2) are all novel findings in this study, that uncovered new anatomical and functional pathways of JGA intercellular communication.

Our results confirmed the well-known microanatomical details of MD cells that have been shown before with TEM and conventional histology approaches. Previous studies revealed the polarized nature of MD epithelium with specific features including the presence of long, apical

primary cilium (Fig. 2C) (7, 31, 32, 36) dilated intercellular spaces (Fig. 5) (16, 17) and unique basal protrusions containing vesicles (Figs. 1-5)(2, 4, 7, 16). Although the presence of MD cell basal processes has been described in these earlier reports, in light of the present findings it appears that the highly extensive nature of these structures has been previously unrecognized or understated. This was likely due to the lack of techniques to study living MD cells, and the inherent technical limitations of TEM to accurately identify the cellular origin and complex 3D structure of these long, interdigitating major and minor processes within the densely packed tissue of the JGA. Of note it is well established that MD cells do not form gap junctions with other cells of the JGA (23, 37) although the importance of intercellular communications in this region is well known. Therefore, the dense network of MD cell processes and vesicle-containing long (up to 30-50 μ m, Figs. 3B, 4A-D and 6C) maculapodia that the present studies visualized projecting towards other MD cells and the glomerular vascular pole in close contact with cells of the mesangium, AA and EA (Fig. 6A-C) may be key ultrastructural elements of MD-to-JGA cell communications.

The exceptional detailed view of the MD microanatomical structure shown in the present study was made possible by the use of a recently established MD-GFP inducible fluorescent reporter mouse model (27) in which MD cells were specifically labeled by high level of membrane-targeted GFP expression. Partial tamoxifen induction in MD-GFP mice enabled the visualization of single MD cells within the multi-cell MD plaque, revealing the fine details of MD cell basolateral features, especially the major and minor cell processes running between individual MD cells (Figs. 1-4). This detailed view is lost when all MD cells within the MD plaque are highly fluorescent (Fig. 1C-D), which necessitated the presently used single cell labeling approach similarly to that in a recent podocyte study (13). Additional technical novelties in the present studies were the high spatial and temporal resolution MPM imaging of intact living MD-GFP

mouse kidney tissues *in vivo* and *in vitro* (Fig. 3A-B), in freshly isolated live single MD cells (Fig. 4), and the use of 3D reconstruction models (Fig. 6). These approaches confirmed that all MD cells under all conditions have major and minor processes, however these structures were not always clearly visible in thin tissue sections due to their intertwined, complex 3D morphology (Fig. 6A). Therefore, due to this inherent limitation of conventional thin tissue sections, the length rather than the number (density) of the longest major processes were clearly visualized and analyzed (Fig. 2G).

Since most MD cell minor processes are tightly packed in the tiny extracellular space at the base of MD cells (Fig. 5D), they were best viewed in isolated single cells (Fig. 4). The membrane labeling in MD cells by targeted GFP expression enabled the visualization of both the plasma (cell processes) and intracellular membranes (vesicles). An additional benefit of this approach combined with live cell imaging was to gain new knowledge of the dynamics of MD processes, such as rapid outgrowth and profound vesicular transport, suggesting their role in MD cell secretory functions in JGA cell-to-cell communications (Fig. 4D, Supplemental Videos S3-4). Despite these advantages of using freshly isolated MD cells, it should be noted that the observed features of MD cell minor processes may not be representative of the *in vivo* behavior of MD cells and may, at least in part, result from the cells' adaptation to *in vitro* culture conditions. In contrast to MD cells in the intact tissue (Fig. 1), no major processes were seen in freshly isolated MD cells (Fig. 4) likely due to remodeling of the actin cytoskeleton. In addition, while MD cell major processes showed no further expansion by dietary salt in female mice (Fig. 2D-G), the number of MD cell minor processes from female mice increased in response to low salt condition (Fig. 4A). Nevertheless, the presence of minor processes was confirmed in intact living MD cells (Figs. 2-3) suggesting that these structures are not artifacts due to *in vitro* culturing. If their ability of rapid

outgrowth as demonstrated here (Fig. 4D, Supplemental Video S3) is preserved in situ (which needs to be confirmed in future work), this would suggest that MD cells can quickly form new connections with other JGA cells.

As suggested in a recent report (7) and present TEM studies (Fig. 5B, D), the dense-core vesicles described in the MD basal processes are likely secretory in nature and may contain a diverse cargo. To identify at least one element of the cargo, we performed immunolabeling for PAPP2, a known secreted protein and local regulator of insulin-like growth factor (IGF) bioavailability, that was localized to the cortical thick ascending limb-distal tubule region in recent reports (8, 20). The expression of PAPP2 in MD cells including within cell processes in a vesicular pattern (Fig. 4D) is further strengthening the secretory role of MD cells in cell-to-cell communication. The role and target JGA cell type of PAPP2 needs further investigation. Similarly, the molecular building blocks of maculapodia, including the presence of actin (Fig. 4C), actin-associated and microtubule proteins, beyond ARHGEF25, ARPC1A, CFAP36, ITF43 that were localized to MD cells based on data from the Human Protein Atlas (not validated in the current work) (Fig. 4C), need to be identified in future studies.

Since the maculapodia network is very likely involved in the MD-to-JGA effector cell communication, the presently observed up-regulation of the length and density of these structures by low dietary salt intake (Figs. 2, 4) may be a structural component of the well-known physiological adaptations in the classic function of MD, namely higher sensitivity of tubuloglomerular feedback control of renal and glomerular hemodynamics, and increased renin secretion under low-salt diet conditions (9, 18, 24, 26). Interestingly, the female gender was another stimulatory factor of both major and minor MD cell processes (Figs. 2G and 4A). While the density of minor processes was up-regulated by both female gender and low-salt diet and ACE inhibitor

treatment (additive effect, Fig. 4A), the length of major processes in control female mice increased to the level of low-salt stimulated condition and did not further increase with low-salt diet and ACE inhibition (Fig. 2G). These results may suggest that the low salt and female regulatory mechanisms likely utilize similar signaling pathways for the control of major but not the minor processes. The gender difference in the length of major processes was preserved in the condition of high dietary salt intake, which had a significant negative effect in both males and females (Fig. 2G). Gender differences identified in these studies further support the notion that in addition to several other kidney functions and mechanisms (19) JGA function is regulated by male and female sex hormones as suggested by previous reports (12, 35). Considering the strategically central localization of MD cells at the glomerular entrance, and the key role these cells play in sensing alterations in the tubular environment and transducing signals to regulate glomerular filtration rate and the activity of the renin-angiotensin system in both health and disease, it is intriguing to speculate that the presently described MD microanatomical features may play a role in gender disparities in kidney disease prevalence and progression (19). The functional relevance of maculapodia in controlling glomerular hemodynamics, vasoactivity, including the functions of PAPP2 and other secreted MD factors on AA and EA renin producing cells and other, yet to be identified renin-negative JGA target cells (Fig. 6C) needs further study.

In summary, the present study illuminated a physiologically regulated dense network of basal cell major and minor processes (maculapodia) in MD cells that were understated in previous work. The newly identified dynamic and secretory features of these microanatomical structures suggest the presence of novel functional and molecular pathways of cell-to-cell communication in the JGA between the MD and other target cells that need to be further explored in future studies.

Detailed characterization of the function and further molecular details of MD cell intercellular communications and their role in physiology and disease warrant further studies.

Grants

This work was supported by US National Institutes of Health grants DK064324, DK123564, and S10OD021833 to J.P-P.

Disclosures

J.P-P. and G.G. are co-founders of Macula Densa Cell LLC, a biotechnology company that develops therapeutics to target macula densa cells for a regenerative treatment for chronic kidney disease. Macula Densa Cell LLC has a pending patent entitled “Targeting macula densa cells as a new therapeutic approach for kidney disease”. J. P-P. received consulting fees from Retrophin and Eli Lilly &Co.

Author contributions

G.G. and J.P.P. designed the study, and wrote the manuscript. U.N.S, A.R.B, W.K., B.K., C.R.N., K.P.A., N.A., I.S.G., J-Y.M., and D.D. made substantial contributions to acquire data. G.G., W.K., B.K., and J.P.P. analyzed the imaging data. All authors approved the final version of the manuscript.

Acknowledgments

U.N.S. was funded by predoctoral research fellowship 19PRE34380886 of the American Heart Association. D.D. was funded by a postdoctoral research fellowship of the Société Francophone du Diabète. C.R.N acknowledges the British Heart Foundation PG/08/059/25335 and K.P.A. the Medical Research Council (MR/P003214/1). The authors would like to thank the help of Dr. T. Starborg at the Wellcome Trust Centre for Cell Matrix Research, University of Manchester, Manchester, UK.

References

1. **Arkill KP, Qvortrup K, Starborg T, Mantell JM, Knupp C, Michel CC, Harper SJ, Salmon AH, Squire JM, Bates DO, and Neal CR.** Resolution of the three dimensional structure of components of the glomerular filtration barrier. *BMC Nephrol* 15: 24, 2014.
2. **Barajas L.** Anatomy of the juxtaglomerular apparatus. *Am J Physiol* 237: F333-343, 1979.
3. **Barajas L.** The juxtaglomerular apparatus: anatomical considerations in feedback control of glomerular filtration rate. *Fed Proc* 40: 78-86, 1981.
4. **Barajas L.** Renin secretion: an anatomical basis for tubular control. *Science* 172: 485-487, 1971.
5. **Barajas L.** The ultrastructure of the juxtaglomerular apparatus as disclosed by three-dimensional reconstructions from serial sections. The anatomical relationship between the tubular and vascular components. *J Ultrastruct Res* 33: 116-147, 1970.
6. **Bell PD, Lapointe JY, and Peti-Peterdi J.** Macula densa cell signaling. *Annu Rev Physiol* 65: 481-500, 2003.
7. **Cangiotti AM, Lorenzi T, Zingaretti MC, Fabri M, and Morroni M.** Polarized Ends of Human Macula Densa Cells: Ultrastructural Investigation and Morphofunctional Correlations. *Anat Rec (Hoboken)* 301: 922-931, 2018.

8. **Cowley AW, Jr., Yang C, Kumar V, Lazar J, Jacob H, Geurts AM, Liu P, Dayton A, Kurth T, and Liang M.** Pappa2 is linked to salt-sensitive hypertension in Dahl S rats. *Physiol Genomics* 48: 62-72, 2016.
9. **Dev B, Drescher C, and Schnermann J.** Resetting of tubulo-glomerular feedback sensitivity by dietary salt intake. *Pflugers Arch* 346: 263-277, 1974.
10. **Fenton RA, and Praetorius J.** Anatomy of the Kidney. In: *Brenner and Rector's The Kidney E-Book*, edited by Yu ASL, Chertow GM, Luyckx V, Marsden PA, Skorecki K, and Taal MWElsevier Health Sciences, 2015, p. pp 42-82.
11. **Fogarty MJ, Hammond LA, Kanjhan R, Bellingham MC, and Noakes PG.** A method for the three-dimensional reconstruction of Neurobiotin-filled neurons and the location of their synaptic inputs. *Front Neural Circuits* 7: 153, 2013.
12. **Fu Y, Lu Y, Liu EY, Zhu X, Mahajan GJ, Lu D, Roman RJ, and Liu R.** Testosterone enhances tubuloglomerular feedback by increasing superoxide production in the macula densa. *Am J Physiol Regul Integr Comp Physiol* 304: R726-733, 2013.
13. **Grgic I, Brooks CR, Hofmeister AF, Bijol V, Bonventre JV, and Humphreys BD.** Imaging of podocyte foot processes by fluorescence microscopy. *J Am Soc Nephrol* 23: 785-791, 2012.
14. **Gyarmati G, Kadoya H, Moon JY, Burford JL, Ahmadi N, Gill IS, Hong YK, Der B, and Peti-Peterdi J.** Advances in Renal Cell Imaging. *Semin Nephrol* 38: 52-62, 2018.
15. **Hackl MJ, Burford JL, Villanueva K, Lam L, Susztak K, Schermer B, Benzing T, and Peti-Peterdi J.** Tracking the fate of glomerular epithelial cells in vivo using serial multiphoton imaging in new mouse models with fluorescent lineage tags. *Nat Med* 19: 1661-1666, 2013.
16. **Kaissling B, and Kriz W.** Variability of intercellular spaces between macula densa cells: a transmission electron microscopic study in rabbits and rats. *Kidney Int Suppl* 12: S9-17, 1982.

17. **Kirk KL, Bell PD, Barfuss DW, and Ribadeneira M.** Direct visualization of the isolated and perfused macula densa. *Am J Physiol* 248: F890-894, 1985.
18. **Komlosi P, Peti-Peterdi J, Fuson AL, Fintha A, Rosivall L, and Bell PD.** Macula densa basolateral ATP release is regulated by luminal [NaCl] and dietary salt intake. *Am J Physiol Renal Physiol* 286: F1054-1058, 2004.
19. **Layton AT, and Sullivan JC.** Recent advances in sex differences in kidney function. *Am J Physiol Renal Physiol* 316: F328-f331, 2019.
20. **Lindstrom NO, De Sena Brandine G, Tran T, Ransick A, Suh G, Guo J, Kim AD, Parvez RK, Ruffins SW, Rutledge EA, Thornton ME, Grubbs B, McMahon JA, Smith AD, and McMahon AP.** Progressive Recruitment of Mesenchymal Progenitors Reveals a Time-Dependent Process of Cell Fate Acquisition in Mouse and Human Nephrogenesis. In: *Dev Cell*. United States: 2018 Elsevier Inc, 2018, p. 651-660 e654.
21. **Lindstrom NO, McMahon JA, Guo J, Tran T, Guo Q, Rutledge E, Parvez RK, Saribekyan G, Schuler RE, Liao C, Kim AD, Abdelhalim A, Ruffins SW, Thornton ME, Baskin L, Grubbs B, Kesselman C, and McMahon AP.** Conserved and Divergent Features of Human and Mouse Kidney Organogenesis. *J Am Soc Nephrol* 29: 785-805, 2018.
22. **Muzumdar MD, Tasic B, Miyamichi K, Li L, and Luo L.** A global double-fluorescent Cre reporter mouse. *Genesis* 45: 593-605, 2007.
23. **Peti-Peterdi J.** Calcium wave of tubuloglomerular feedback. *Am J Physiol Renal Physiol* 291: F473-480, 2006.
24. **Peti-Peterdi J, and Harris RC.** Macula densa sensing and signaling mechanisms of renin release. *J Am Soc Nephrol* 21: 1093-1096, 2010.

25. **Peti-Peterdi J, Kidokoro K, and Riquier-Brison A.** Novel in vivo techniques to visualize kidney anatomy and function. *Kidney Int* 88: 44-51, 2015.
26. **Peti-Peterdi J, Komlosi P, Fuson AL, Guan Y, Schneider A, Qi Z, Redha R, Rosivall L, Breyer MD, and Bell PD.** Luminal NaCl delivery regulates basolateral PGE2 release from macula densa cells. *J Clin Invest* 112: 76-82, 2003.
27. **Riquier-Brison ADM, Sipos A, Prokai A, Vargas SL, Toma L, Meer EJ, Villanueva KG, Chen JCM, Gyarmati G, Yih C, Tang E, Nadim B, Pendekanti S, Garrelds IM, Nguyen G, Danser AHJ, and Peti-Peterdi J.** The macula densa prorenin receptor is essential in renin release and blood pressure control. *Am J Physiol Renal Physiol* 315: F521-f534, 2018.
28. **Schiessl IM, Fremter K, Burford JL, Castrop H, and Peti-Peterdi J.** Long-Term Cell Fate Tracking of Individual Renal Cells Using Serial Intravital Microscopy. *Methods Mol Biol* 2019.
29. **Schnermann J.** Homer W. Smith Award lecture. The juxtaglomerular apparatus: from anatomical peculiarity to physiological relevance. *J Am Soc Nephrol* 14: 1681-1694, 2003.
30. **Shroff UN, Schiessl IM, Gyarmati G, Riquier-Brison A, and Peti-Peterdi J.** Novel fluorescence techniques to quantitate renal cell biology. *Methods Cell Biol* 154: 85-107, 2019.
31. **Sipos A, Vargas S, and Peti-Peterdi J.** Direct demonstration of tubular fluid flow sensing by macula densa cells. *Am J Physiol Renal Physiol* 299: F1087-1093, 2010.
32. **Song J, Wang L, Fan F, Wei J, Zhang J, Lu Y, Fu Y, Wang S, Juncos LA, and Liu R.** Role of the Primary Cilia on the Macula Densa and Thick Ascending Limbs in Regulation of Sodium Excretion and Hemodynamics. *Hypertension* 70: 324-333, 2017.
33. **Taugner R, Schiller A, Kaissling B, and Kriz W.** Gap junctional coupling between the JGA and the glomerular tuft. *Cell Tissue Res* 186: 279-285, 1978.

34. Uhlén M, Fagerberg L, Hallström BM, Lindskog C, Oksvold P, Mardinoglu A, Sivertsson Å, Kampf C, Sjöstedt E, Asplund A, Olsson I, Edlund K, Lundberg E, Navani S, Szgyarto CA, Odeberg J, Djureinovic D, Takanen JO, Hober S, Alm T, Edqvist PH, Berling H, Tegel H, Mulder J, Rockberg J, Nilsson P, Schwenk JM, Hamsten M, von Feilitzen K, Forsberg M, Persson L, Johansson F, Zwahlen M, von Heijne G, Nielsen J, and Pontén F. Proteomics. Tissue-based map of the human proteome. *Science* 347: 1260419, 2015.
35. Veiras LC, Girardi ACC, Curry J, Pei L, Ralph DL, Tran A, Castelo-Branco RC, Pastor-Soler N, Arranz CT, Yu ASL, and McDonough AA. Sexual Dimorphic Pattern of Renal Transporters and Electrolyte Homeostasis. *J Am Soc Nephrol* 28: 3504-3517, 2017.
36. Wang L, Shen C, Liu H, Wang S, Chen X, Roman RJ, Juncos LA, Lu Y, Wei J, Zhang J, Yip KP, and Liu R. Shear stress blunts tubuloglomerular feedback partially mediated by primary cilia and nitric oxide at the macula densa. *Am J Physiol Regul Integr Comp Physiol* 309: R757-766, 2015.
37. Yao J, Oite T, and Kitamura M. Gap junctional intercellular communication in the juxtaglomerular apparatus. *Am J Physiol Renal Physiol* 296: F939-946, 2009.

Figure legends

Figure 1. Histological features of the MD-GFP mouse model. A: Overview of a MD-GFP mouse kidney section with membrane-targeted eGFP expression in MD cells (green, arrowheads), and membrane-targeted tdTomato expression in all other kidney cell types (red). Nuclei are labeled with DAPI (blue). Note that all green cells are localized directly adjacent to intensely red labeled

glomeruli (G). **B:** Immunofluorescence double labeling of the MD cell marker nNOS (red) and the nNOS-driven eGFP reporter (green). The overlay image shows co-localization (yellow) confirming MD-specific expression of eGFP. **C-D:** Fluorescence images of MD-GFP mouse kidney sections showing longitudinal, horizontal, and cross sectional view of the MD cell plaque after full (C) or partial (D) induction of eGFP expression by tamoxifen. Some images show tissue autofluorescence (C, blue) for additional morphological detail. Note the fine morphological details of single MD cells that are visible only with partial tamoxifen induction, that include major (arrowhead) and minor cell processes (arrows) at the cell base, projecting towards the glomerulus and other MD cells (D). Dashed circle represents the border of the MD plaque. G: glomerulus, MD: macula densa, IA: interlobular arteriole, AA: afferent arteriole. Bars are 20 μ m.

Figure 2. Representative images and morphological analysis of MD cell major processes. A-E: Native fluorescence images of MD plaques from MD-GFP kidney frozen sections with single, eGFP-labeled MD cells and the adjacent glomerulus. Note the increased length of major cell processes (arrowheads) compared to control (A) in conditions of low-salt diet with ACE inhibition (B), but the much shorter length of these structures in high-salt diet (C). Occasionally, the primary cilium of MD cells was visible at the apical membrane (C, arrow). Compared to kidney tissue from male mice (A-C), MD cell major processes were more elaborate in female mice (D-F). **F:** High magnification maximum projection image of a z-stack series of optical sections showing a maculapodia network consisting of major (arrowhead) and minor processes (arrows) in a single MD cell (same area magnified as shown in panel E). **G:** Statistical summary showing the alterations in the length of MD cell major processes based on gender and in response to various dietary salt intake conditions (33-100 total data points in each group, n=4 in all groups except n=5

in female low-salt diet with ACE inhibition). **: $P < 0.01$, ns=not significant compared to control in same gender group. Comparisons between male and female genders of same salt diet groups are shown by bars. ****: $P < 0.0001$. G: glomerulus, MD: macula densa, CTRL: control, LS+ACEi: low-salt diet with ACE inhibition, HS: high-salt diet. H: Representative image of eGFP-labeled MD cells from a deep juxtamedullary (JM) nephron. Note the presence of major cell processes (arrowheads) similarly to MD cells from superficial cortical nephrons (A-F). Bars are 20 μm .

Figure 3. MPM imaging of maculapodia in intact living kidney tissues.

A-B: Representative MPM z-stack (Supplemental Video S1) projection images of a low-salt diet and ACE inhibitor treated MD-GFP mouse kidney in vivo (A) and in the freshly isolated and in vitro microperfused JGA preparation (B). Note the MD cell-specific eGFP expression (green) and tdTomato expression in all other kidney cell types (red). Plasma was labeled by Albumin-Alexa Fluor 680 (grey) in panel A. Nuclei are labeled with DAPI (blue) in panel B. The MD areas are magnified in both panels as indicated with labeling of MD cell major (arrowheads) and minor processes (arrows). Dashed circle represents the border of MD plaque. G: glomerulus, MD: macula densa, cTAL: cortical thick ascending limb, EA: efferent arteriole, AA: afferent arteriole. Bars are 20 μm .

Figure 4. Representative images of the regulation (A), and structural and dynamic features (B-D) of MD cell minor processes.

A: Representative images and statistical summary of the long, thin, hairlike minor cell processes of living, eGFP-labeled MD cells freshly isolated from male and female animals in control condition (n=3 male and female each) or after combined low-salt diet with ACE inhibition (n=4 male and n=3 female) as labeled (A). Note the high density of very

long MD cell processes in female LS+ACEi panel (arrow)(also in Supplemental Video S2). Variability in cell body appearance (presence/absence of dark nuclear region) is due to different z-planes of optical sections. **B:** Comparison of MD cell (eGFP, green) and control cell (tdTomato, red) membrane structures in freshly isolated single cells or cell groups. Note the presence of numerous long, minor processes in MD cells (green) in a group of 3 cells that remained attached to each other, but not in control (red) cells. Minor processes (arrows) were seen only at basal cell regions, identified based on anatomical considerations and the typical apical location of MD cell nuclei. **C:** Immunofluorescence labeling of alpha-tubulin (green) and F-actin (red) in freshly isolated and attached MD cells (note the presence of F-actin but not tubulin in minor processes (arrows)) and immunoperoxidase labeling of actin associated proteins Rho Guanine Nucleotide Exchange Factor 25 (ARHGEF25) and Actin Related Protein 2/3 Complex Subunit 1A (ARPC1A), Cilia Flagella Associated Protein 36 (CFAP36) and Intraflagellar Transport Protein 43 (IFT43) showing high level and MD cell-specific expression in human kidney tissue. Magnified insets show labeling at the MD apical (arrowheads) and basal membranes (arrows).

Immunoperoxidase images are from the Human Protein Atlas, and available for ARHGEF25 (https://images.proteinatlas.org/52016/120419_A_8_5.jpg), ARPC1A (https://images.proteinatlas.org/4334/13143_A_8_5.jpg), CFAP36 (https://images.proteinatlas.org/8994/24077_A_7_5.jpg), and IFT43 (https://images.proteinatlas.org/3438/10487_A_8_5.jpg).

D: Structural and dynamic features of MD cell minor processes including multiple vesicles visible within the processes (arrows, high GFP intensity) in a freshly isolated eGFP-expressing single MD cell (also in Supplemental Video S4); immunofluorescence image of Pregnancy-Associated Plasma Protein A2 (PAPPA2) expression in the human kidney showing high level of labeling in

MD cells (red) in a vesicular pattern including at basal cell regions (red arrows) (autofluorescence is shown in green, cell nuclei are labeled blue with DAPI) with inset demonstrating the lack of PAPP2 immunolabeling after blocking with the immunizing peptide; PAPP2 immunofluorescence labeling (red) in fixed freshly isolated attached MD cells showing vesicular pattern within cell processes (magnified inset, arrows); time-lapse imaging of a freshly isolated eGFP-expressing single MD cell showing rapid outgrowth of minor processes (arrow) within 2 minutes (also in Supplemental Video S3). G: Glomerulus, MD: Macula Densa, CTRL: control condition, LS+ACEi: low-salt diet with ACE inhibition. Bars are 10 μ m.

Figure 5. Transmission electron microscopy (A-D) and serial block-face scanning electron microscopy (E) images of the MD cell basal region ultrastructure in the rabbit (A-B), rat (C-D), and human kidney (E). **A:** Overview of a rabbit MD plaque. The profile of eight MD cells can be distinguished based on the presence of apical tight junctions (5 of these cells have visible cell nuclei). The lateral intercellular spaces are expanded. The interface to the extraglomerular mesangium (EGM) displays processes from MD cells that appear to protrude into the area. One of the MD cells with a prominent basal major process is highlighted in yellow. Other basal major and minor processes that seem to interdigitate with each other and cannot be clearly assigned to a certain cell are marked by red arrows. **B:** The cell with its prominent major process shown in panel A (yellow) is enlarged showing that from the trunk of the major process many fine ramifications (minor processes) emerge. Such processes may contain dark staining vesicles (red arrow). **C:** Slightly tangential section through the MD and the EGM of a rat kidney. The lateral intercellular spaces are expanded. MD cells are interconnected by minor processes (arrows, magnified in inset). The interface between the MD and EGM consists of an area with many cell processes of MD cells

that are intertwined with each other (partially separated by basement membrane material) and seem to protrude into the EGM. **D:** Cross-section of a MD plaque in rat kidney shows the extensive MD basal cell major and minor processes network. The MD basal processes are crossing the fragmented basement membrane (black arrows) and protruding into the EGM. The magnified inset shows the tangential and cross sections of minor processes that contain several vesicles of variable density (red arrows). **E:** Overview of a MD and adjacent EGM region in human kidney. Several MD cells can be distinguished. The lateral intercellular spaces are expanded. MD cells appear to have a high density of basal cell processes (arrows) running towards the EGM as well as to the branching EA. MD: Macula Densa, EGM: Extraglomerular mesangium, EA: Efferent Arteriole. Bars are 10 μm .

Figure 6. Visualization of MD cell basal major and minor processes in 3D in the MD-GFP mouse kidney. Reconstruction of a MD plaque and the adjacent glomerulus, afferent (AA), and efferent (EA) arterioles in 3D from a female MD-GFP mouse receiving low salt diet and ACE inhibition. **A:** Whole-mount immunofluorescence labeling of optically cleared mouse kidney tissue using CLARITY. MD cells were identified with GFP labeling (green), and the basement membrane was labeled with collagen IV immunostaining (magenta). Cell nuclei were labeled with DAPI (blue). 3D surface rendering revealed the network of MD cell basal major and minor processes running towards the EGM, the AA and the EA (arrows). **B-C:** Immunofluorescence labeling and optical sectioning of 20 μm thick frozen sections of MD-GFP mouse kidney. Three MD cells (MD1-3) were labeled by the endogenous, membrane targeted eGFP (green), and juxtaglomerular renin cells were visualized by renin immunolabeling (magenta). Z-stack maximum intensity projection image of the vascular pole of a glomerulus including the AA and

EA, and in-between the MD (B). C: 3D reconstruction with surface rendering analysis of the same xyz image as shown in panel B. The smooth eGFP⁺ areas are the 3 MD cells' apical surfaces (arrows). Surface rendering model enabled the visualization of the fine details of the dense MD cell basal processes network and the anatomical orientation of the basal cell major and minor processes of MD cells (arrowheads) relative to the EGM, AA and EA. Note the dense network of MD cell minor processes and their long extensions (up to 30 μ m) projecting towards renin-labeled (magenta) individual cells of the AA and EA, as well as towards renin-negative cells of the EGM. Bar is 10 μ m for all panels.

Figure 1

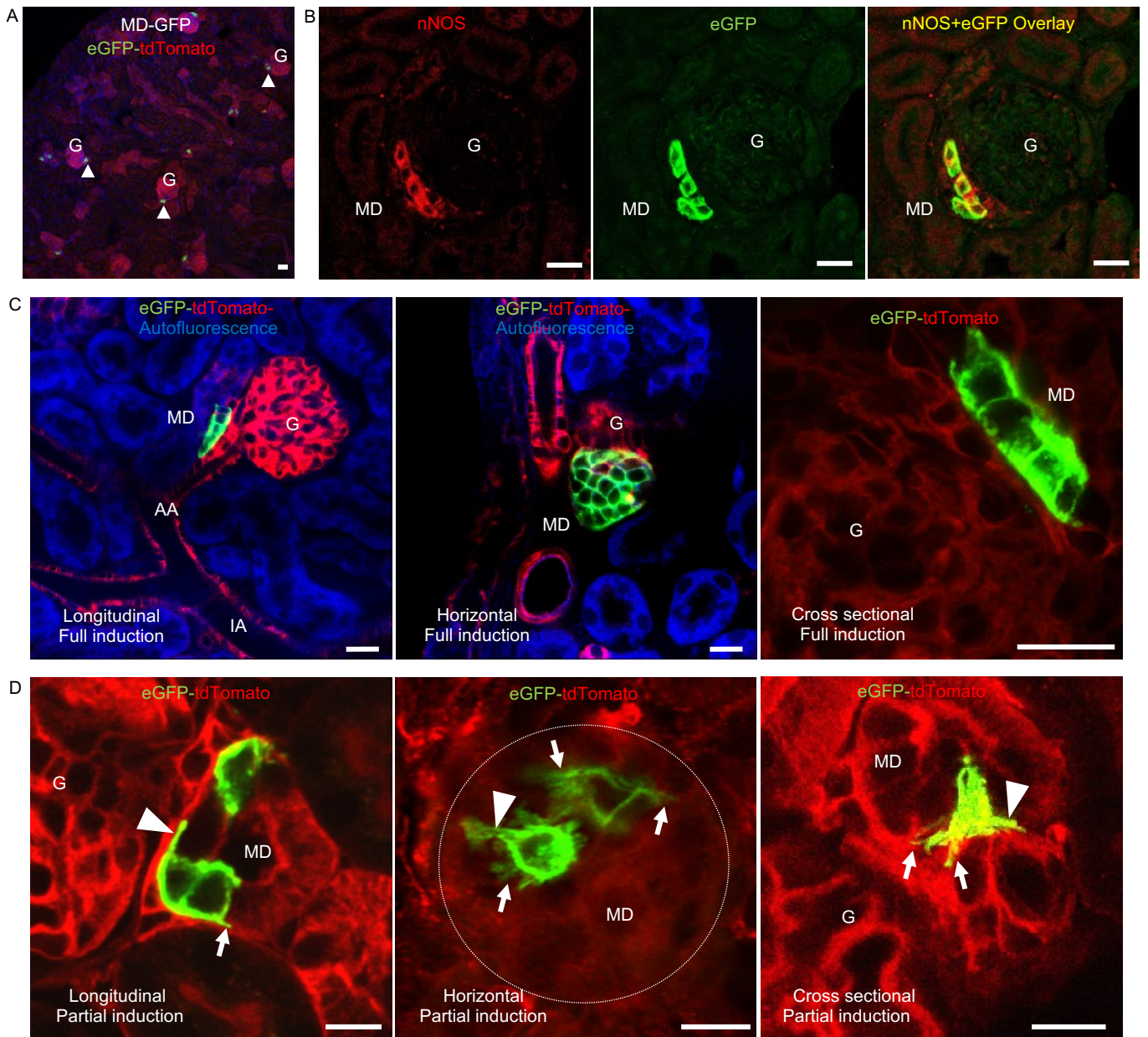


Figure 2

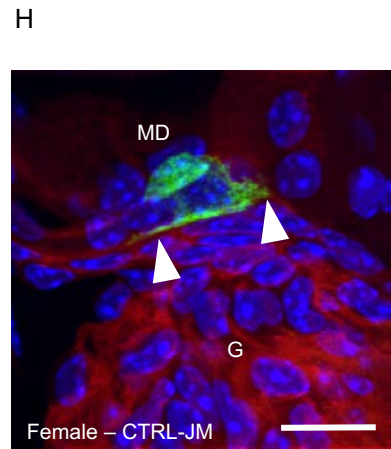
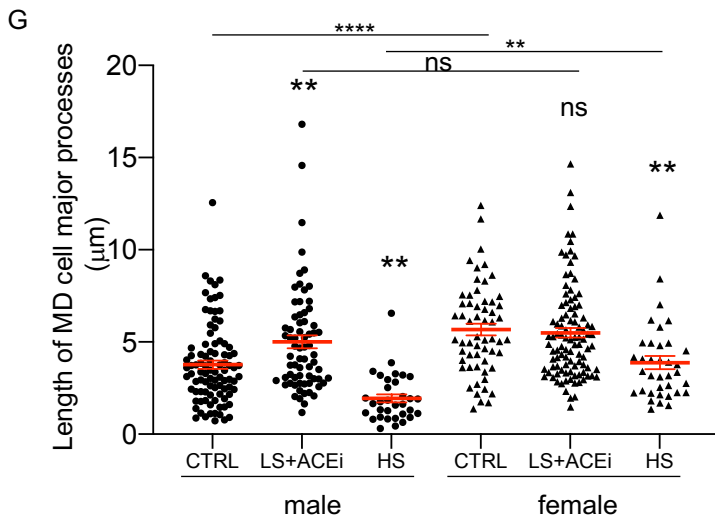
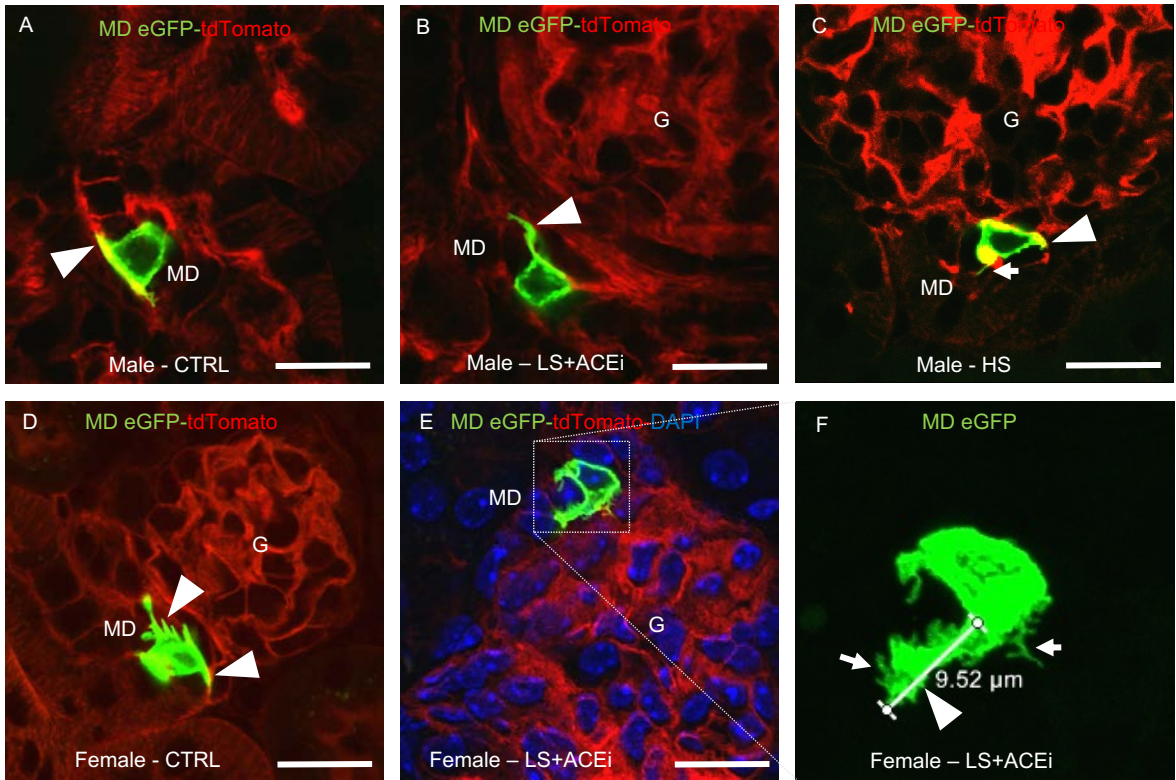


Figure 3

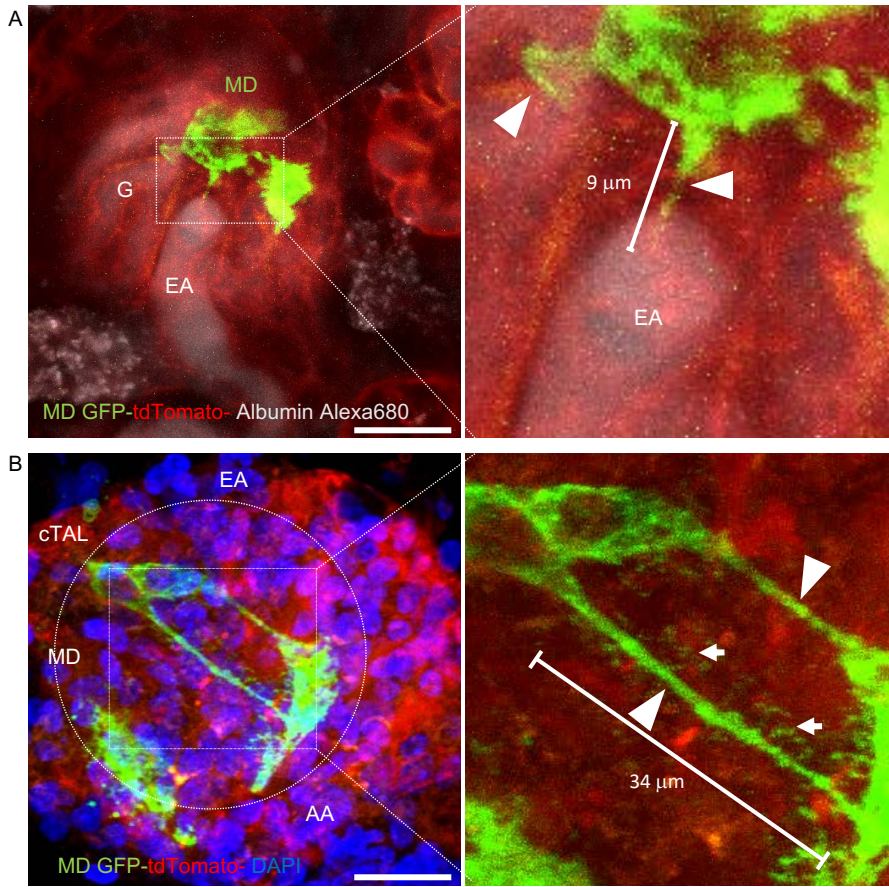


Figure 4

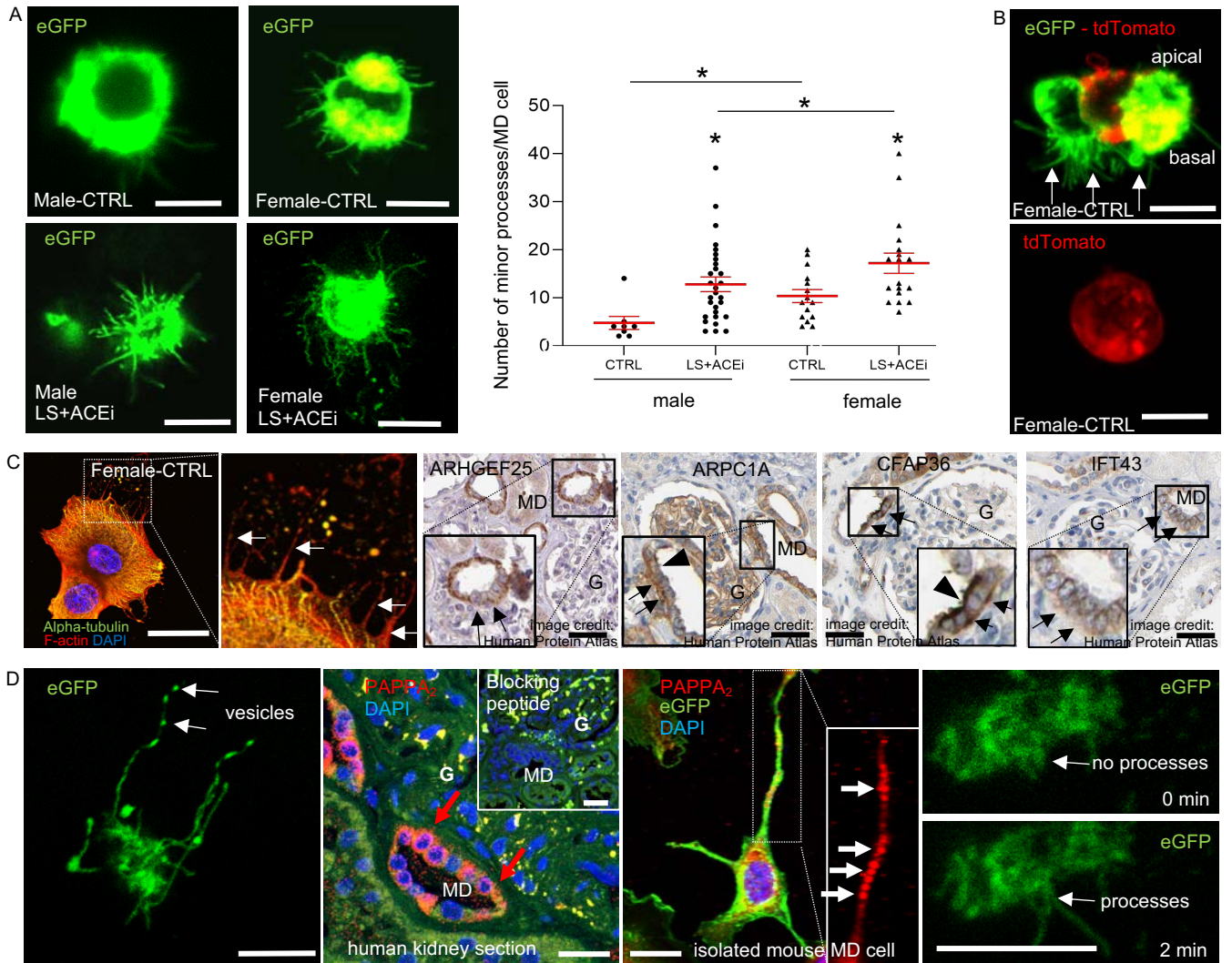


Figure 5

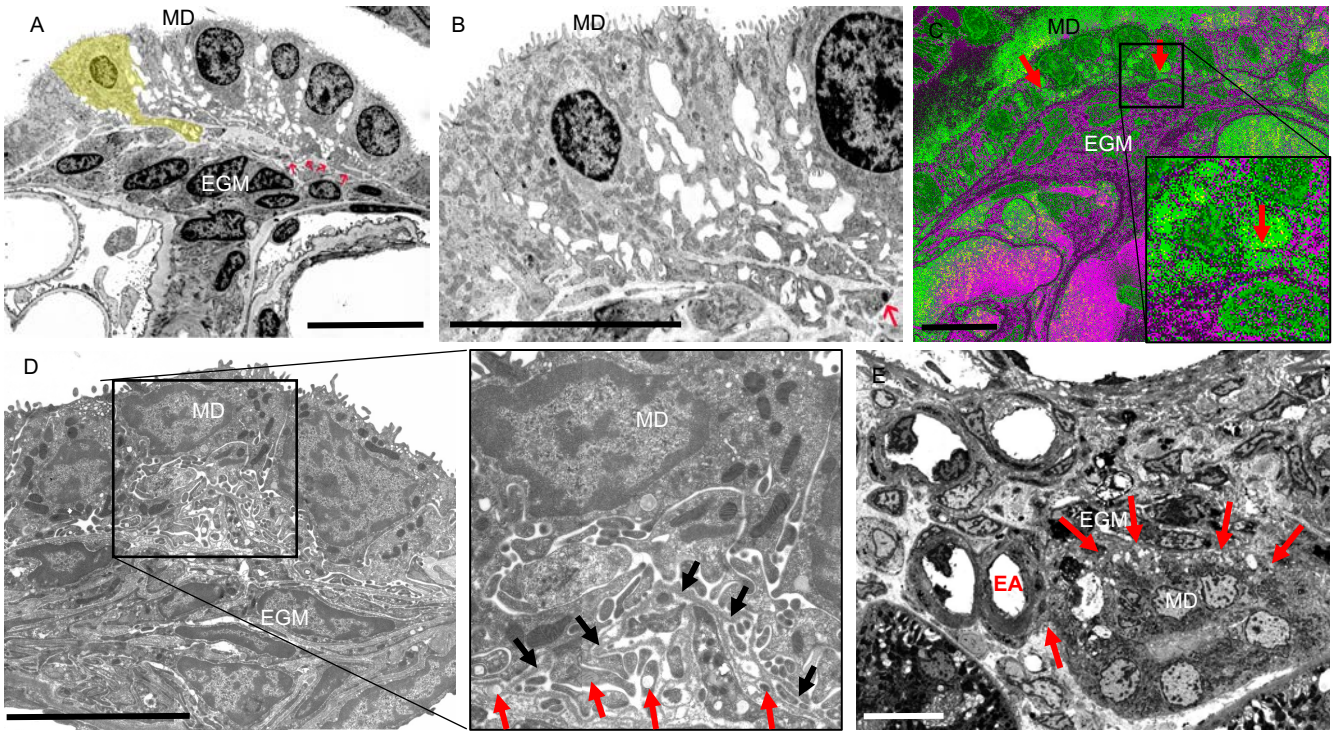


Figure 6

